

Multi-source quantitative PAT in diffusive regime

Guillaume Bal* Kui Ren†

May 30, 2011

Abstract

Photoacoustic tomography (PAT) is a novel hybrid medical imaging technique that aims to combine the large contrast of optical coefficients with the high resolution capabilities of ultrasound. We assume that the first step of PAT, namely the reconstruction of a map of absorbed radiation from ultrasound boundary measurement, has been done. We focus on quantitative photoacoustic tomography (QPAT), which aims at quantitatively reconstructing the optical coefficients from knowledge of the absorbed radiation map.

We present a non-iterative procedure to reconstruct such optical coefficients, namely the diffusion and absorption coefficients, and the Grüneisen coefficient when the propagation of radiation is modeled by a second-order elliptic equation. We show that PAT measurements allow us to uniquely reconstruct only two out of the above three coefficients, even when data are collected using an arbitrary number of radiation illuminations. We present uniqueness and stability results for the reconstructions of such two parameters and demonstrate the accuracy of the reconstruction algorithm with numerical reconstructions from two-dimensional synthetic data.

Key words. Quantitative photoacoustic tomography, hybrid imaging modality, hybrid inverse problem, interior data, diffusion regime, non-iterative reconstruction.

1 Introduction

Photoacoustic tomography (PAT) is a recent *hybrid* medical imaging modality that combines the large contrast of optical parameters with the high resolution capabilities of ultrasonic waves. Optical tomography is an imaging modality that utilizes the large contrast observed in optical parameters. Its spatial resolution is, however, limited because of multiple scattering of light [6, 7]. Ultrasound exhibits much lower contrast because sound speeds vary little between healthy and unhealthy tissues. However, the focusing of ultrasonic waves allows for high resolution reconstructions. PAT is based on the photo-acoustic effect, which couples

*Department of Applied Physics and Applied Mathematics, Columbia University, New York, NY 10027; gb2030@columbia.edu

†Department of Mathematics, University of Texas at Austin, One University Station C1200, Austin, TX 78712; ren@math.utexas.edu

optical and ultrasonic waves in a way that may be described as follows. As optical radiation propagates, a fraction of its energy is absorbed and generates a local heating of the underlying medium. The resulting mechanical expansion is the source of acoustic signals that propagate through the domain of interest. Ultrasonic transducers located at the boundary of the domain then record the emitted pressure waves as a function of time.

A first inverse problem in PAT consists of reconstructing the absorbed radiation map $H(x)$ from the pressure measurements. For reference to this inverse problem in the physical and engineering literatures, we refer the reader to, e.g., [17, 23, 40, 41] and their references. When sound speed is constant, explicit formulas have been obtained for a large class of geometries of interest; see [21, 22, 29, 30, 35] and their references. When sound speed is not constant but known, time reversal algorithms perform well under standard non-trapping conditions as demonstrated in [5, 27, 38]. Note that acoustic absorption is typically neglected in such reconstructions. Accounting for absorption is in fact a difficult and not entirely understood problem [28].

In this paper, we assume that the above first step is done and that $H(x)$ is known. The absorbed radiation map $H(x)$ is proportional to the absorption coefficient $\sigma(x)$, the intensity $u(x)$ of the radiation that reaches the point x , and the Grüneisen coefficient $\Gamma(x)$, which measures how much ultrasound is generated by the absorbed radiation. The second step of PAT, called quantitative photoacoustics (QPAT), aims to reconstruct the unknown optical parameters and the Grüneisen coefficient from knowledge of $H(x) = \Gamma(x)\sigma(x)u(x)$. For QPAT in the setting of transport equations, we refer the reader to [8]. We consider here the case where radiation propagation is modeled by a second-order elliptic (diffusion) equation. The unknown coefficients are (D, σ, Γ) , the diffusion, absorption, and Grüneisen coefficients, respectively.

QPAT may be done in several ways. Radiating fields (photons) propagating with different optical frequencies (colors) do not interact with one another and thus solve uncoupled equations. Since the optical coefficients themselves depend on color, one methodology consists of using multiple radiation illuminations (this is the multi-source setting) and acquire as many radiation maps $H(x)$. The objective is then to reconstruct the unknown parameters independently for each color of interest. This is the setting considered in e.g., [12, 37, 42] and in this paper. Alternatively, a second methodology is to probe the domain of interest at multiple optical wavelengths (colors) and to reconstruct optical coefficients based on prior information regarding their frequency dependence [9, 17, 18]; see also [19] for a different QPAT in the presence of chromophores with intensity-dependent absorption properties. We refer the reader to [9] for an extension of the work presented in this paper to the setting where prior information on the frequency dependence of the unknown coefficients is taken into account.

This paper has two main objectives. In [12], the Grüneisen coefficient is assumed to be known. In that setting, it is then shown that two *well chosen illuminations* are sufficient to uniquely and stably reconstruct (D, σ) . Moreover, [12] provides an explicit method to solve (D, σ) that relies on solving a *transport equation* and a *second-order elliptic equation*. The well-posedness of the transport equation requires that a vector field constructed from available data satisfy appropriate assumptions. The set of *well-chosen illuminations* that guaranty such assumptions is based on the construction of complex geometric optics solutions

and is not very explicit. The *first objective* of this paper is to show that a large class of illuminations allows for stable and robust reconstructions of (D, σ) in the two-dimensional setting and to implement (a modified version of) the reconstruction proposed in [12] and obtain robust and stable numerical reconstructions of (D, σ) for a large class of illuminations.

The *second objective* of the paper is to generalize the method in [12] to the reconstruction of the three parameters (D, σ, Γ) . There, we show a somewhat *negative* result: no matter how many illuminations are used and how many corresponding $H(x)$ are constructed, the available data allow us to reconstruct only two functionals of (D, σ, Γ) . The two functionals uniquely determine all possible measurements of the form $H(x) = \Gamma(x)\sigma(x)u(x)$. Thus, independent of any method of reconstruction, two well-constructed measurements (H_1, H_2) uniquely characterize all other possible measurements of the form $H(x)$ and there is therefore no need to acquire them, at least in the setting of noise-free data. However, we prove the positive result that these two functionals uniquely characterize any pair of coefficients in (D, σ, Γ) *provided* that the third one is known. These results are summarized in Theorem 2.2 and Corollary 2.3 below.

Section 2 devoted to the presentation of the theoretical results also provides a new stability estimate for the solution to the transport equation. Under the assumption that the vector field in the transport equation does not vanish, we obtain Hölder estimates for the solution to the transport equation in different L^p norms in terms of errors in the measurement $H(x)$ also in L^q norms. (A function $f(x)$ is in $L^p(X)$ of a domain X when $\|f\|_p^p := \int_X |f(x)|^p dx < \infty$.) These results are summarized in Theorem 2.4 and are based on a direct analysis of the transport equation, as in e.g. [2], rather than on the method of characteristics as in [12].

The practical difficulties inherent to the numerical simulation of the transport and elliptic equations that appear in QPAT are described in section 3. Several numerical experiments presented in section 4 show the robustness of solving the transport and elliptic equations to reconstruct two possibly highly oscillatory coefficients in (D, σ, Γ) from measurements of the form $H(x) = \Gamma(x)\sigma(x)u(x)$. We also show that increasing the number of illuminations, which is unnecessary in the presence of noise-free data, allows us to obtain more stable reconstructions of two coefficients in the presence of noisy data when the third coefficient is known. This is consistent with the better stability estimates obtained in [12] in the presence of multiple illuminations.

Let us finally mention that QPAT is one example in a large family of hybrid inverse problems where one aims at reconstructing coefficient from knowledge of internal data. For similar inverse problems with internal data that have been addressed in the mathematical literature, we refer the reader to, e.g., [4, 10, 11, 14, 31, 32, 33, 39].

2 Reconstruction formulas and stability results

In Quantitative photoacoustic tomography (QPAT) in the diffusive regime, photon (radiation) propagation is modeled by the following second-order elliptic equation

$$\begin{aligned} -\nabla \cdot D(x)\nabla u + \sigma(x)u &= 0 \quad \text{in } X \\ u &= g \quad \text{on } \partial X, \end{aligned} \tag{1}$$

with prescribed Dirichlet conditions at the boundary ∂X . Throughout the paper, we assume that X is a bounded open domain in \mathbb{R}^d with smooth boundary ∂X . The optical coefficients $(D(x), \sigma(x))$ with $D(x)$ the diffusion coefficient and $\sigma(x)$ the absorption coefficient are assumed to be bounded from above and below by positive constants. In the theoretical analyses below, we also assume that they are Lipschitz continuous, i.e., of class $W^{1,\infty}(X)$ (the space of differentiable functions with bounded derivative).

The information about the coefficients in QPAT takes the following form:

$$H(x) = \gamma(x)u(x) \quad \text{a.e. } x \in X, \quad \text{where } \gamma(x) := \Gamma(x)\sigma(x). \quad (2)$$

The coefficient $\Gamma(x)$ is the Grüneisen coefficient. In many works in QPAT, it is assumed to be constant. We assume here that it is Lipschitz continuous and bounded above and below by positive constants.

The objective of QPAT is to reconstruct (D, σ, Γ) from knowledge of $H(x)$ in (2) obtained for a given number of illuminations g in (1). The main results of this paper are that:

- Two well chosen illuminations provide two independent relations $\chi = \chi(D, \sigma, \Gamma)$ and $q = q(D, \sigma, \Gamma)$ of the three coefficients (D, σ, Γ) . This allows us to uniquely reconstruct two out of the three coefficients (D, σ, Γ) provided the third one is known.
- These two independent relations uniquely determine the measurements $H(x)$ for all other possible illuminations $g(x)$ on ∂X . In other words, independent of the number of illuminations and corresponding measurements, all that we can reconstruct about (D, σ, Γ) is (χ, q) . This makes it impossible to reconstruct the three coefficients (D, σ, Γ) from QPAT data without additional prior information.
- For two well-chosen illuminations, the reconstruction of (χ, q) is Hölder-stable, which means that an error of order ϵ in the data in an appropriate norm generates an error in the reconstruction of (χ, q) of order ϵ^κ in another appropriate norm for some $\kappa > 0$. (We say that a reconstruction is Lipschitz-stable when $\kappa = 1$.)

Our main assumptions are that:

- (i) The coefficients (D, σ, Γ) are of class $W^{1,\infty}(X)$ and bounded above and below by positive constants. The coefficients (D, σ, Γ) are known on ∂X .
- (ii) The illuminations g_1 and g_2 are positive functions on ∂X and we assume that they are the values (the restrictions) on ∂X of functions of class $C^3(\bar{X})$ (i.e., functions that are three times differentiable with continuous derivative of order 3 on $\bar{X} = X \cup \partial X$).
- (iii) the vector field

$$\beta := H_1 \nabla H_2 - H_2 \nabla H_1 = H_1^2 \nabla \frac{H_2}{H_1} = H_1^2 \nabla \frac{u_2}{u_1} = -H_2^2 \nabla \frac{H_1}{H_2} \quad (3)$$

is a vector field in $W^{1,\infty}(X)$ such that

$$|\beta|(x) \geq \alpha_0 > 0, \quad \text{a.e. } x \in X. \quad (4)$$

By standard regularity theory for elliptic equations and the maximum principle [25], the solutions to (1) are of class $W^{3,p}(X)$. Here and below, we denote by $W^{m,p}(X)$ the space of functions with derivatives of order less than or equal to m in $L^p(X)$.

Beyond the regularity assumptions on (D, σ, Γ) , the domain X , and the boundary conditions g_1 and g_2 , the only real assumption we impose is (4). In general, there is no guaranty that the gradient of $\frac{u_2}{u_1}$ does not vanish. The existence of vector fields such that (4) holds independent of the unknown coefficients (D, σ, Γ) in a large set of coefficients is proved in [12]. In that paper, illuminations that are close to values on ∂X of specific complex geometric optics (CGO) solutions are shown to be sufficient to ensure (4). The proof in [12] displays sufficient conditions for (4) to hold. However, such conditions are far from being necessary and in fact many vector fields not based on the CGO solutions still satisfy (4).

In dimension $d = 2$, a simple condition guarantees that (4) holds. We have the following result [2, 32]:

Lemma 2.1. *Assume that $h = \frac{g_2}{g_1}$ on ∂X is an almost two-to-one function in the sense of [32], i.e., a function that is a two-to-one map except possibly at its minimum and at its maximum. Then (4) is satisfied.*

Proof. Upon multiplying the equation for u_1 by u_2 , the equation for u_2 by u_1 , and subtracting both relations, we obtain

$$\begin{aligned} -\nabla \cdot (Du_1^2) \nabla \frac{u_2}{u_1} &= 0, \quad \text{in } X \\ \frac{u_2}{u_1} &= \frac{g_2}{g_1}, \quad \text{on } \partial X. \end{aligned} \tag{5}$$

This implies that $v := \frac{u_2}{u_1}$ satisfies an elliptic equation with a diffusion coefficient $\tilde{D} = Du_1^2$ bounded from above and below by positive constants. Note that $\beta = H_1^2 \nabla v$. Results in, e.g., [2, Theorem 1.2] show that ∇v cannot vanish inside X . By the maximum principle and the assumption on h , no critical point of v can occur on ∂X either. This implies that $|\nabla v| > 0$ and that we can find a constant such that (4) holds since H_1^2 is bounded from below by a positive constant and by continuity $|\nabla v|$ attains its (strictly positive) minimum in \bar{X} . \square

In dimension $d \geq 3$, the above result on the (absence of) critical points of elliptic solutions no longer holds. However, by continuity, we may verify that (4) is satisfied for a large class of illuminations when D is close to a constant and σ is sufficiently small. For arbitrary coefficients (D, σ) in dimension $d \geq 3$, the only available proof that (4) is satisfied for an open set of illuminations is the one obtained in [12]. Note also that (4) is a sufficient condition for us to solve the inverse problem of QPAT. In [2], a similar problem is addressed in dimension $d = 2$ without assuming a constraint of the form (4). In this paper, we consider vector field for which (4) holds.

Uniqueness result. We first prove a result that provides uniqueness up to a specified transformation.

Theorem 2.2. *Assume that hypotheses (i)-(iii) hold. Then*

(a) $H_1(x)$ and $H_2(x)$ uniquely determine the whole measurement operator $\mathcal{H} : H^{\frac{1}{2}}(\partial X) \rightarrow H^1(X)$, which to g defined on ∂X associates $\mathcal{H}(g) = H$ in X defined by (2).

(b) The measurement operator \mathcal{H} uniquely determines the two following functionals of (D, σ, Γ) :

$$\chi(x) := \frac{\sqrt{D}}{\Gamma\sigma}(x), \quad q(x) := -\left(\frac{\Delta\sqrt{D}}{\sqrt{D}} + \frac{\sigma}{D}\right)(x). \quad (6)$$

Here Δ is the Laplace operator.

(c) Knowledge of the two functionals χ and q uniquely determines $H_1(x)$ and $H_2(x)$. In other words, the reconstruction of (D, σ, Γ) is unique up to transformations that leave (χ, q) invariant.

Proof. Let us start with (a). As in the derivation of (5), we obtain

$$\begin{aligned} -\nabla \cdot (Du_1^2) \nabla \frac{H_2}{H_1} &= 0, & \text{in } X \\ Du_1^2 &= D|_{\partial X} g_1^2, & \text{on } \partial X. \end{aligned} \quad (7)$$

This is a transport equation in conservative form for Du_1^2 . More precisely, this is a transport equation $\nabla \cdot \rho \tilde{\beta} = 0$ for ρ with $\rho|_{\partial X} = 1$ and $\tilde{\beta} = \chi^2 \beta = (Du_1^2) \nabla \frac{H_2}{H_1}$. Since $\tilde{\beta} \in W^{1,\infty}(X)$ and is divergence free, the above equation for ρ admits the unique solution $\rho \equiv 1$ since (4) holds. Indeed, we find that $\nabla \cdot (\rho - 1)^2 \tilde{\beta} = 0$ by application of the chain rule with $\rho|_{\partial X} - 1 = 0$ on ∂X . Upon multiplying the equation by $\frac{H_2}{H_1}$ and integrating by parts, we find

$$\int_X (\rho - 1)^2 \chi^2 H_1^2 \left| \nabla \frac{H_2}{H_1} \right|^2 dx = 0.$$

Using (4), we deduce that $\rho \equiv 1$. This proves that Du_1^2 is uniquely determined. Dividing by $H_1^2 = (\Gamma\sigma)^2 u_1^2$, this means that $\chi > 0$ is uniquely determined. Note that we do not need the full $W^{1,\infty}(X)$ regularity of β . All we need is that β be sufficiently regular so that the *renormalization property* holds in order to obtain the above integral; see [3, 13, 16, 20]. However, we still need a condition of the form (4) to conclude that the solution to the transport equation is unique. See in particular the treatment of two-dimensional vector fields in [15, 26].

Let now g be an arbitrary boundary condition and let u be the solution to (1) and $H = \mathcal{H}g$ defined by (2). Replacing H_2 above by H yields

$$\begin{aligned} -\nabla \cdot \chi^2 H_1^2 \nabla \frac{H}{H_1} &= 0, & \text{in } X \\ H &= \Gamma|_{\partial X} \sigma|_{\partial X} g, & \text{on } \partial X. \end{aligned} \quad (8)$$

This is a well-defined elliptic equation with a unique solution $H \in H^1(X)$ for $g \in H^{\frac{1}{2}}(\partial X)$. This proves that \mathcal{H} is uniquely determined by (H_1, H_2) .

Let us next prove (b). We have already seen that χ was determined by (H_1, H_2) , which is clearly determined by \mathcal{H} . Moreover, define $v = \sqrt{D}u_1$, which is also uniquely determined based on the results in (a). Define

$$q = \frac{-\Delta v}{v} = -\frac{\Delta(\sqrt{D}u_1)}{\sqrt{D}u_1}.$$

Since u_1 is bounded from below, is sufficiently smooth, and solves (1), a routine calculation shows that q is given by (6).

Finally, we prove (c). Since q is known, we can solve

$$(\Delta + q)v_j = 0, \quad X, \quad v_j = \sqrt{D_{|\partial X}}g_j \quad \partial X, \quad j = 1, 2.$$

Because q is of the specific form (6) as a prescribed functional of (D, σ, Γ) , it is known that $(\Delta + q)$ does not admit 0 as a (Dirichlet) eigenvalue, for otherwise, 0 would also be a (Dirichlet) eigenvalue of the elliptic operator

$$(-\nabla \cdot D\nabla + \sigma) \cdot = (-\sqrt{D}(\Delta + q)\sqrt{D}) \cdot. \quad (9)$$

The latter calculation is the standard Liouville transformation allowing us to replace an elliptic operator by a Schrödinger operator. Thus v_j is uniquely determined for $j = 1, 2$. Now,

$$H_j = \Gamma \sigma u_j = \frac{\Gamma \sigma}{\sqrt{D}} v_j = \frac{v_j}{\chi}, \quad j = 1, 2,$$

and is therefore uniquely determined by (χ, q) . □

On the reconstruction of two coefficients. The above result shows that the unique reconstruction of (D, σ, Γ) is not possible even from knowledge of the full measurement operator \mathcal{H} defined in Theorem 2.2. We therefore face this peculiar situation that two well-chosen illuminations uniquely determine the functionals (χ, q) but that acquiring additional measurements does not provide any new information, at least in the absence of noise in the data. However, if one coefficient in (D, σ, Γ) is known, then we have the following positive result that the other two coefficients are uniquely determined:

Corollary 2.3. *Under the hypotheses of the previous theorem, let (χ, q) in (6) be known. Then*

- (a) *If Γ is known, then (D, σ) are uniquely determined.*
- (b) *If D is known, then (σ, Γ) are uniquely determined.*
- (c) *If σ is known, then (D, Γ) are uniquely determined.*

Proof. (a) is probably the most practical case as Γ is often assumed to be constant. Since Γ is known, then so is $\Gamma\chi = \sqrt{D}/\sigma$ so that we have the elliptic equation for \sqrt{D} :

$$(\Delta + q)\sqrt{D} + \frac{1}{\Gamma\chi} = 0, \quad X, \quad \sqrt{D_{|\partial X}} = \sqrt{D_{|\partial X}}, \quad \partial X. \quad (10)$$

Again, because of the specific form of q , $(\Delta + q)$ is invertible and the above equation admits a unique solution. Once \sqrt{D} , hence D , is known, then so is $\sigma = \frac{\sqrt{D}}{\Gamma\chi}$.

If D is known in (b), then σ is known from q and Γ is known from χ .

Finally in (c), we obtain that from the expression for q that

$$\sqrt{D}(\Delta + q)\sqrt{D} + \sigma = 0 \quad X, \quad \sqrt{D}|_{\partial X} = \sqrt{D}|_{\partial X}, \quad \partial X. \quad (11)$$

We need to prove a uniqueness result for the above nonlinear equation for \sqrt{D} . Let us assume that \sqrt{D} and another solution $\tau\sqrt{D}$ for $0 < \tau(x)$ satisfy the above equation for σ fixed. We have

$$-\sqrt{D}(\Delta + q)\sqrt{D}\tau - \frac{\sigma}{\tau} = 0 \quad X.$$

Thanks to (9), this implies the following equation for τ :

$$-\nabla \cdot D\nabla\tau + \sigma\left(\tau - \frac{1}{\tau}\right) = 0, \quad X, \quad \tau = 1, \quad \partial X.$$

Upon multiplying by $\tau - 1$ and integrating by parts, we find that

$$\int_X D|\nabla(\tau - 1)|^2 dx + \int_X \sigma|\tau - 1|^2 \frac{\tau + 1}{\tau} dx = 0.$$

Since $\tau > 0$, we deduce from the above that $\tau \equiv 1$ and that D is uniquely determined by q . We then retrieve Γ from knowledge of χ . \square

Reconstruction formulas. Note that the above uniqueness results are *constructive*. In all cases, we need to solve the transport equation for χ :

$$-\nabla \cdot (\chi^2\beta) = 0 \quad \text{in } X, \quad \chi|_{\partial X} \text{ known on } \partial X, \quad (12)$$

with β the vector field defined in (3). This uniquely defines $\chi > 0$. Then we find that

$$q(x) = -\frac{\Delta(H_1\chi)}{H_1\chi} = -\frac{\Delta(H_2\chi)}{H_2\chi}. \quad (13)$$

This provides explicit reconstructions for (χ, q) . In case (b), no further equation needs to be solved. In cases (a) and (c), we need to solve an elliptic equation for \sqrt{D} , which is the linear equation (10) in (a) and the nonlinear equation (11) in (c). These are the steps that will be implemented in the sections on numerical simulations below.

Stability of the solution of the transport equation. Before presenting our numerical framework, we derive a stability result for the reconstruction of χ . A similar result was obtained in [12] by using the stability of the method of characteristics to solve ordinary differential equations. Here, we present a stability result that is directly obtained from the PDE (7) and is similar in spirit to estimates obtained in [2] and to the notion of renormalization property of transport equation [20]. Similar stability results can be obtained for q and then for (D, σ, Γ) depending on the reconstruction considered.

Theorem 2.4. *We assume that the hypotheses of Theorem 2.2 hold. Let $H = (H_1, H_2)$ be the measurements corresponding to the coefficients (D, σ, Γ) for which hypothesis (iii) holds. Let $\tilde{H} = (\tilde{H}_1, \tilde{H}_2)$ be the measurements corresponding to the same illuminations (g_1, g_2) with another set of coefficients $(\tilde{D}, \tilde{\sigma}, \tilde{\Gamma})$ such that (i) and (ii) still hold. Then we find that*

$$\|\chi - \tilde{\chi}\|_{L^p(X)} \leq C \|H - \tilde{H}\|_{(W^{1, \frac{p}{2}}(X))^2}^{\frac{1}{2}}, \quad \text{for all } 2 \leq p < \infty. \quad (14)$$

Let us assume, moreover, that $\gamma(x)$ is of class $C^3(\bar{X})$. Then we have the estimate

$$\|\chi - \tilde{\chi}\|_{L^p(X)} \leq C \|H - \tilde{H}\|_{(L^{\frac{p}{2}}(X))^2}^{\frac{1}{3}}, \quad \text{for all } 2 \leq p < \infty. \quad (15)$$

By interpolation [1], the latter result implies that

$$\|\chi - \tilde{\chi}\|_{L^\infty(X)} \leq C \|H - \tilde{H}\|_{(L^{\frac{p}{2}}(X))^2}^{\frac{p}{3(d+p)}}, \quad \text{for all } 2 \leq p < \infty. \quad (16)$$

We may for instance choose $p = 4$ above to measure the noise level in the measurement H in the square integrable norm when noise is described by its power spectrum in the Fourier domain.

Proof. Define $\nu = \chi^2$ and $\tilde{\nu} = \tilde{\chi}^2$ with χ defined in (6) and β and $\tilde{\beta}$ as in (3). Then we find that

$$\nabla \cdot \frac{\nu - \tilde{\nu}}{\nu}(\nu\beta) + \nabla \cdot \tilde{\nu}(\beta - \tilde{\beta}) = 0.$$

Note that $\nu\beta = \chi^2 H_1^2 \nabla \frac{H_2}{H_1}$ is a divergence-free field. Let φ be a twice differentiable, non-negative, function from \mathbb{R}^1 to \mathbb{R} with $\varphi(0) = \varphi'(0) = 0$. Then we find that

$$\nabla \cdot \varphi\left(\frac{\nu - \tilde{\nu}}{\nu}\right)(\nu\beta) + \varphi'\left(\frac{\nu - \tilde{\nu}}{\nu}\right) \nabla \cdot \tilde{\nu}(\beta - \tilde{\beta}) = 0.$$

Let us multiply this equation by a test function $\zeta \in H^1(X)$ and integrate by parts. Since $\nu = \nu'$ on ∂X , we find

$$\int_X \varphi\left(\frac{\nu - \tilde{\nu}}{\nu}\right) \nu\beta \cdot \nabla \zeta dx + \int_X \tilde{\nu}(\beta - \tilde{\beta}) \nabla \cdot \left[\zeta \varphi'\left(\frac{\nu - \tilde{\nu}}{\nu}\right)\right] dx = 0.$$

Upon choosing $\zeta = \frac{H_2}{H_1}$, we find

$$\int_X \varphi \nu H_1^2 \left| \nabla \frac{H_2}{H_1} \right|^2 dx + \int_X \tilde{\nu}(\beta - \tilde{\beta}) \cdot \nabla \frac{H_2}{H_1} \varphi' dx + \int_X \tilde{\nu}(\beta - \tilde{\beta}) \cdot \nabla \frac{\nu - \tilde{\nu}}{\nu} \frac{H_2}{H_1} \varphi'' dx = 0.$$

Above, φ stands for $\varphi\left(\frac{\nu - \tilde{\nu}}{\nu}\right)$ in all integrals. By assumption on the coefficients, $\nabla \frac{\nu - \tilde{\nu}}{\nu}$ is bounded a.e.. This is one of our main motivations for assuming that the optical coefficients are Lipschitz. The middle term is seen to be smaller than the third term and so we focus on the latter one. Upon taking $\varphi(x) = |x|^p$ for $p \geq 2$ and using assumption (iii), we find that

$$\|\nu - \tilde{\nu}\|_{L^p(X)}^p \leq C \int_X |\beta - \tilde{\beta}| |\nu - \tilde{\nu}|^{p-2} dx.$$

By an application of the Hölder inequality, we deduce that

$$\|\nu - \tilde{\nu}\|_{L^p(X)} \leq C \|\beta - \tilde{\beta}\|_{L^{\frac{p}{2}}(X)}^{\frac{1}{2}}.$$

We next write $\beta - \tilde{\beta} = (H_1 - \tilde{H}_1)\nabla H_2 + \tilde{H}_1(\nabla(H_2 - \tilde{H}_2) - \dots$ and use the fact that the solutions to (1) and the coefficients are in $W^{1,\infty}(X)$ to conclude that (14) holds.

The other results are obtained by regularity theory and interpolation. Indeed from regularity results in [25] with coefficients in $W^{1,\infty}(X)$, we find that the solutions to (1) are of class $W^{3,q}(X)$ for all $1 \leq q < \infty$. Since the coefficient γ is of class $C^3(\bar{X})$, then the measurements H_j are of class $W^{3,q}(X)$ for all $1 \leq q < \infty$. Standard Sobolev estimates [25] show that

$$\|H_j - \tilde{H}_j\|_{W^{1,q}(X)} \leq C \|H_j - \tilde{H}_j\|_{L^q(X)}^{\frac{2}{3}} \|H_j - \tilde{H}_j\|_{W^{3,q}(X)}^{\frac{1}{3}}.$$

The last term is bounded by a constant, which gives (15) for $q = \frac{p}{2}$. Another interpolation result states that

$$\|\varphi\|_{\infty} \leq \|\nabla\varphi\|_{\infty}^{\theta} \|\varphi\|_p^{1-\theta}, \quad \theta = \frac{d}{d+p}.$$

This provides the stability result in the uniform norm (16). \square

On the reconstruction of one coefficient. We conclude our theoretical section by the reconstruction of one coefficient when the other two coefficients are known. This is significantly simpler than the reconstruction of two coefficients. In none of the cases do we need to solve a transport equation involving the vector field β . The latter was obtained by eliminating σ from the elliptic equation, which is no longer necessary when two coefficients are already known.

When only Γ is unknown, then we solve (1) for u and then construct $\Gamma = \frac{H}{\sigma u}$.

When only σ is unknown, then we solve

$$\begin{aligned} -\nabla \cdot D\nabla u(\mathbf{x}) + \frac{H}{\Gamma} &= 0, & \text{in } X \\ u(\mathbf{x}) &= g(\mathbf{x}), & \text{on } \partial X \end{aligned}, \quad \sigma = \frac{H}{\Gamma u}. \quad (17)$$

When only D is unknown, we obtain $u = \frac{H}{\sigma\Gamma}$ and then the above elliptic equation in (17) with $D|_{\partial X}$ known is a transport equation for D . As soon as ∇u is a sufficiently smooth, non-vanishing vector field, then D is uniquely determined by the above linear equation. This problem is analyzed in e.g., [2, 36].

3 Numerical implementation of the reconstruction

In this section and the next, we present a numerical implementation of the reconstruction procedure given in the above theorem and its corollary. We recall that we have to solve a transport equation to reconstruct χ and q and an elliptic equation to reconstruct D when the latter is not known.

All the theoretical results require a certain degree of smoothness of the coefficients we are interested in. The numerical experiments below show that the reconstructions are quite robust even when the coefficients display multiple jump singularities. When this occurs, the numerical implementation has to be done carefully in order to avoid spurious oscillations.

Numerical simulation of the transport equations. The reconstruction procedure we presented above is non-iterative in the sense that the nonlinear inverse problem is solved in one step. No iterations or updating of the unknowns are necessary as in the nonlinear reconstruction schemes used in optical tomography [6]. In principle, we only need to solve the transport equation (7) numerically to reconstruct $\chi^2 = Du_1^2/H_1^2$. In practice, we have to be careful in the numerical computations because the vector field $\beta = H_1^2 \nabla \frac{H_2}{H_1}$ usually varies significantly over the domain. We found it numerically useful to normalize the vector field in the transport equation (7). We rewrite the transport equation as

$$\begin{aligned} -\nabla \cdot (\chi^2 |\beta|) \hat{\beta} &= 0 && \text{in } X \\ \chi^2 |\beta| &= \frac{\sqrt{D|_{\partial X}}}{\Gamma|_{\partial X} \sigma|_{\partial X}} && \text{on } \partial X, \end{aligned} \quad (18)$$

so that the new vector field $\hat{\beta} = \frac{\beta}{|\beta|}$ is a unit vector everywhere.

Regularization in the presence of noise. When the illuminations are chosen so that the vector field β is regular enough, we can solve (18) directly to reconstruct χ (since $|\beta|$ is known). When the data are noisy, the vector field β computed by differentiating $\frac{H_2}{H_1}$ may become irregular. Solving the transport equation (18) with such an irregular vector field can be problematic in practice. Two ways to regularize the problem have been considered.

The first way of regularizing the problem is to add a small artificial diffusion ε to the transport equation:

$$\begin{aligned} -\varepsilon \Delta (\chi^2 |\beta|) - \nabla \cdot (\chi^2 |\beta|) \hat{\beta} &= 0, && \text{in } X \\ \chi^2 |\beta| &= \frac{\sqrt{D|_{\partial X}}}{\Gamma|_{\partial X} \sigma|_{\partial X}}, && \text{on } \partial X. \end{aligned} \quad (19)$$

We then solve this regularized equation to reconstruct χ .

The second way to regularize the problem is to work directly on the discretized system. We discretize the equation using a first order upwind discontinuous Galerkin method. Let us denote by \mathbf{f} the discretized version of $\chi^2 |\beta|$, \mathbf{A} the corresponding discretized transport operator and \mathbf{d} the right hand side that comes from the boundary condition. We then obtain a system of equations $\mathbf{A}\mathbf{f} = \mathbf{d}$. We solve the transport equation in the least-square sense by minimizing the following functional

$$\mathcal{O}(\mathbf{f}) = \mathcal{F}(\mathbf{f}) + \mathcal{R}(\mathbf{f}) \equiv \frac{1}{2} \|\mathbf{A}\mathbf{f} - \mathbf{d}\|_2^2 + \rho \|\mathbf{M}\mathbf{f}\|_1. \quad (20)$$

Here \mathbf{M} denotes the discretized version of the gradient operator. We have chosen the regularization term to be the TV norm of \mathbf{f} (i.e. l^1 norm of $\mathbf{M}\mathbf{f}$) to deal with discontinuous coefficients. To recover smooth coefficients, we should replace the l^1 norm with the square of the l^2 norm of $\mathbf{M}\mathbf{f}$, $\rho\|\mathbf{M}\mathbf{f}\|_2^2$, in which case the least-square problem admits the explicit solution $\mathbf{f} = (\mathbf{A}^*\mathbf{A} + \rho\mathbf{M}^*\mathbf{M})^{-1}\mathbf{A}^*\mathbf{d}$.

To minimize the objective functional (20) with the l^1 regularization term, we use the Bregman iteration scheme proposed in [34]. The Bregman iteration scheme is characterized by the following iterative procedure for $k \geq 0$ starting with the projection operator \mathcal{P}_0 :

$$\begin{aligned}\mathbf{f}_{k+1} &= \arg \min_{\mathbf{f}} \mathcal{F}(\mathbf{f}) + \mathcal{R}(\mathbf{f}) - \langle \mathcal{P}_k, \mathbf{f} \rangle \\ \mathcal{P}_{k+1} &= \mathcal{P}_k - \nabla_{\mathbf{f}} \mathcal{F}(\mathbf{f}_{k+1}),\end{aligned}\tag{21}$$

where $\nabla_{\mathbf{f}} \mathcal{F}(\mathbf{f}_{k+1})$ means the evaluation of $\nabla_{\mathbf{f}} \mathcal{F}$ at \mathbf{f}_{k+1} . It is proved in [34] that the iterations are well-defined and that the scheme converges if there are only non-smooth functions in the kernel of \mathbf{A} , or at the continuous level, in the kernel of the transport operator with vector field $\hat{\beta}$. For applications of the Bregman method to photoacoustic tomography, see also [24].

Setting with multiple illuminations and construction of vector fields. It is shown in [12] that acquiring $2n$ measurements for well-chosen illuminations can improve the stability of the reconstructions. The main idea is that two measurements allow us to obtain the transport equation considered before: $\nabla \cdot \chi^2 \beta = 0$ so that $\beta \cdot \nabla \chi^2 + \chi^2 \nabla \cdot \beta = 0$ while $2n$ measurements (or sometimes possibly less) allow us to get an equation for the full gradient $\nabla \chi^2$ provided that n linearly independent vector fields can be constructed at each $x \in X$. Instabilities that may appear when solving $\beta \cdot \nabla \chi^2 + \chi^2 \nabla \cdot \beta = 0$ in the vicinity of ∂X when β is almost tangent to ∂X no longer appear when we solve a system of the form $\nabla \chi^2 + \Lambda \chi^2 = 0$ with Λ an appropriate known vector.

We have not tried to implement a reconstruction based on solving the above redundant vectorial equation. However, we have demonstrated that acquiring more measurements was unsurprisingly beneficial when noise was present in the data. In the presence of $I > 2$ data sets, we can write down $I - 1$ transport equations of the form (7) for the same unknown χ but different vector field β_i , $i = 2, \dots, I$. We may then solve the over-determined system of $I - 1$ transport equations to reconstruct χ . We can either solve the system in the least square sense or solve (18) for different indices and then take the average of the results. We can also use multiple data sets as follows. We divide the data into two groups, H_i , $i = 1, \dots, k$ and H_j , $j = k + 1, \dots, I$. We then construct the data $\tilde{H}_1 = \sum_{i=1}^k H_i$ and $\tilde{H}_2 = \sum_{j=k+1}^I H_j$. This is equivalent to saying that \tilde{H}_1 and \tilde{H}_2 are generated by the illuminations $\tilde{g}_1 = \sum_{i=1}^k g_i$ and $\tilde{g}_2 = \sum_{j=k+1}^I g_j$, respectively. Numerically, we have observed that both ways of utilizing multiple data sets yielded almost identical reconstruction results.

Elliptic equation with non-smooth diffusion coefficient. The inversion procedure presented in the theoretical section can be applied to the reconstruction of discontinuous diffusion coefficients. Instead of solving (10) for \sqrt{D} , we reconstruct non-smooth coefficients D as follows. We rewrite the diffusion equation, again using the fact that we can reconstruct

$v_1 = \sqrt{D}u_1$, and $H_1 = \Gamma\sigma u_1$, as

$$\begin{aligned} -\nabla \cdot v_1^2 \nabla \frac{1}{u_1} &= \frac{H_1}{\Gamma}, & \text{in } X, \\ \frac{1}{u_1} &= \frac{1}{g_1}(\mathbf{x}), & \text{on } \partial X. \end{aligned} \tag{22}$$

This is an elliptic equation for $\frac{1}{u_1}$. In the case when $g_1 > 0$ everywhere on ∂X , (22) provides stable reconstructions of u_1 and thus \sqrt{D} , provided that v_1 has been reconstructed faithfully.

4 Simulation results

In all the simulations below, we take the domain of interest to be the square $X = (0, 2)^2$. We use the notation $\mathbf{x} = (x, y)$ and ∂X_L , ∂X_R , ∂X_T , and ∂X_B denote the left, right, top and bottom parts of the boundary, respectively.

We discretize the diffusion equations, such as (1), (11) and (22), and the transport equations, such as (18), with a first-order discontinuous Galerkin method. The domains are covered with triangular finite element meshes with about 15000 nodes. All the plots are displayed on a structured grid interpolating the quantities defined on the finite element mesh with a MATLAB interpolation algorithm. The semilinear elliptic equation (11) is solved with a standard Newton method. We observed that the Newton scheme converged rapidly and was quite robust with respect to changes in the initial guess.

In all the numerical simulations, we construct the interior data $H(x)$ by solving the diffusion equation with the true coefficients on an extremely fine finite element mesh, evaluating $\Gamma\sigma u$ on the fine mesh, and interpolating it onto the coarser mesh used in the reconstructions. The data constructed this way thus contain some “noise” due to the mesh difference and interpolation. Nonetheless, we shall refer to these data as the “noise-free” data. We estimated that this “noise” level was less than 0.2%.

A simple noise model. We also perform reconstructions using noisy data. For want of a more physically realistic noise model, here we simply add a discrete (on the coarse mesh composed of 15000 nodes) i.i.d. noise to the data set $H(\mathbf{x})$ so that

$$\tilde{H}(\mathbf{x}) = H(\mathbf{x}) * (1 + \alpha \text{random}(\mathbf{x})), \tag{23}$$

where $\text{random}(\mathbf{x})$ is an uncorrelated random field taking values in $[-1, 1]$ and α controls the noise level. Such a noise is sufficient to generate highly oscillatory vector fields that complicate the simulation of the transport equation. When sufficiently noisy data are acquired, we need to run a de-noising process on the vector field, which we chose as a low-pass filter constructed by a 5-point sliding averaging process. Although this may not be the best denoising process available, it worked quite well numerically to remove the high-frequency noise generated in (23). A more systematic study of noise in QPAT, including low-frequency noise that may have a larger impact on the reconstructions, still needs to be done.

We measure the quality of the reconstruction using the relative L^2 error between reconstructed and true coefficients. We use \mathcal{E}_σ^C and \mathcal{E}_σ^N to denote the relative L^2 error in the reconstruction of σ from “clean” and “noisy” data, respectively. All noisy data have 8% random noise constructed as in (23).

Vector fields with different illumination patterns. We show here that many pairs of illuminations can generate vector fields that connect every point inside the domain with a point on the boundary of the domain, in the sense that for every point inside the domain, there is an integral curve of the vector field passing through that point and reaching the boundary.

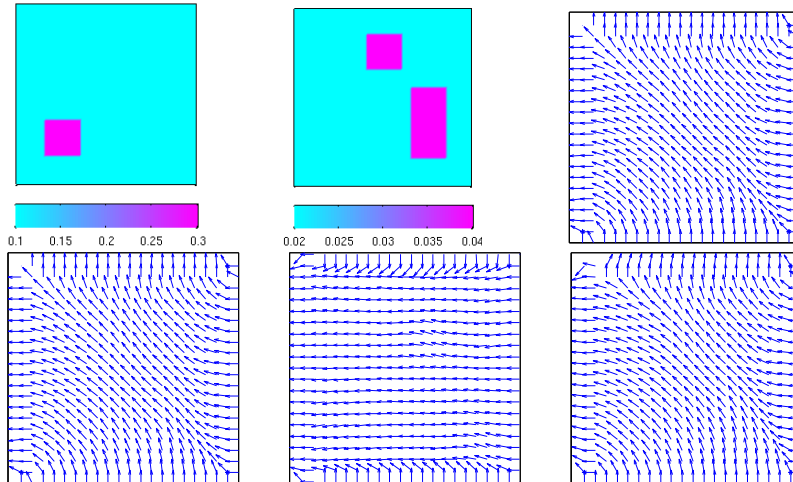


Figure 1: Top left to bottom right: the absorption coefficient, the diffusion coefficient, and the normalized vector fields constructed using the illumination pairs (g_1, g_2) , (g_3, g_4) , (g_5, g_6) , (g_7, g_8) in Experiment 1.

Experiment 1. In the first numerical experiment, we plot the vector fields generated from different pair of illuminations for a problem with the following discontinuous absorption and diffusion coefficients:

$$\sigma(\mathbf{x}) = \begin{cases} 0.3, & \mathbf{x} \in X_1 \\ 0.1, & \mathbf{x} \in X \setminus X_1 \end{cases} \quad D(\mathbf{x}) = \begin{cases} 0.04, & \mathbf{x} \in X_2 \cup X_3 \\ 0.02, & \mathbf{x} \in X \setminus (X_2 \cup X_3), \end{cases}$$

where the inclusions are $X_1 = [0.3 \ 0.7] \times [0.3 \ 0.7]$, $X_2 = [0.8 \ 1.2] \times [1.3 \ 1.7]$ and $X_3 = [1.3 \ 1.7] \times [0.3 \ 1.1]$. The Grüneisen coefficient is taken to be constant and equals 0.5 although it does not play a role in the plot of the vector field. We consider four different pairs of

illuminations (g_1, g_2) , (g_3, g_4) , (g_5, g_6) and (g_7, g_8) that are defined respectively as follows.

$$\begin{aligned}
 g_1 &= \begin{cases} 1.0, & \mathbf{x} \in \partial X_T \cup \partial X_L, \\ 0.5, & \mathbf{x} \in \partial X_B \cup \partial X_R \end{cases} & g_2 &= \begin{cases} 0.5, & \mathbf{x} \in \partial X_T \cup \partial X_L, \\ 1.0, & \mathbf{x} \in \partial X_B \cup \partial X_R \end{cases} \\
 g_3 &= \begin{cases} 1.0, & \mathbf{x} \in \partial X_T \cup \partial X_L, \\ 0.0, & \mathbf{x} \in \partial X_B \cup \partial X_R \end{cases} & g_4 &= \begin{cases} 0.0, & \mathbf{x} \in \partial X_T \cup \partial X_L, \\ 1.0, & \mathbf{x} \in \partial X_B \cup \partial X_R \end{cases} \\
 g_5 &= \begin{cases} 1.0, & \mathbf{x} \in \partial X_L, \\ 0.0, & \mathbf{x} \in \partial X_R \cup \partial X_T \cup \partial X_B \end{cases} & g_6 &= \begin{cases} 0.0, & \mathbf{x} \in \partial X_L \cup \partial X_T \cup \partial X_B, \\ 1.0, & \mathbf{x} \in \partial X_R \end{cases} \\
 g_7 &= \begin{cases} x, & \mathbf{x} \in \partial X_T, \\ y, & \mathbf{x} \in \partial X_L, \\ 0.0, & \mathbf{x} \in \partial X_B \cup \partial X_R \end{cases} & g_8 &= \begin{cases} 0.0, & \mathbf{x} \in \partial X_T \cup \partial X_L, \\ x, & \mathbf{x} \in \partial X_B, \\ y, & \mathbf{x} \in \partial X_R \end{cases}
 \end{aligned}$$

The results of the numerical experiment are shown in Fig. 1. Even though slight errors may occur near boundaries, in general the constructed vector fields are quite accurate. Note that for better visualization purpose, we have plotted the vector field on a mesh that is 8 times coarser than the mesh used in the numerical reconstructions shown below.

Numerical simulations with smooth coefficients. We present in Experiments 2, 3 and 4 the reconstructions of (Γ, σ) , (Γ, D) , and (σ, D) in the setting of smooth coefficients.

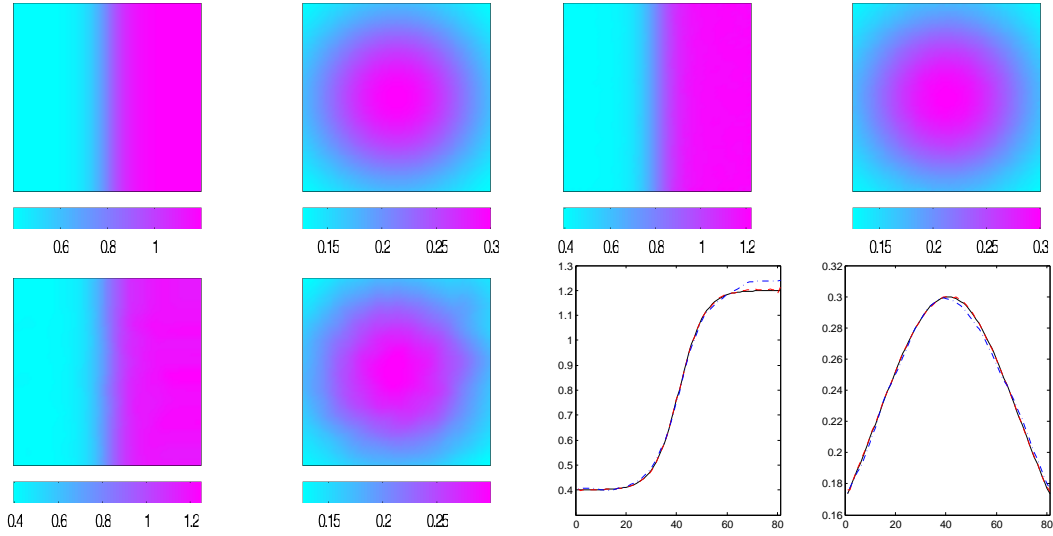


Figure 2: Experiment 2. From top left to bottom right: true Γ and σ , reconstructed Γ and σ with noise-free data, reconstructed Γ and σ with noisy data, cross-section of true (solid) and reconstructed (red dashed and blue dot-dashed) Γ and σ along $y = 1$ with noisy data.

Experiment 2. In this experiment, we intend to reconstruct the Grüneisen and absorption coefficients:

$$\Gamma(\mathbf{x}) = 0.8 + 0.4 \tanh(4x - 4) \quad \text{and} \quad \sigma(\mathbf{x}) = 0.1 + 0.2e^{-(x-1)^2 - (y-1)^2}.$$

The diffusion coefficient is a known constant $D(\mathbf{x}) = 0.01 + 0.01 \tanh(4y - 4)$. The measurements are constructed with the two sources g_1 and g_2 . The results of the numerical experiment are shown in Fig. 2. The accuracy of the reconstructions can be best seen in the cross-section plots. The relative L^2 errors, defined as the ratio between the L^2 error in a reconstructed image and L^2 norm of the corresponding true image, in the reconstructions are $\mathcal{E}_\Gamma^C = 0.2\%$, $\mathcal{E}_\Gamma^N = 1.1\%$, $\mathcal{E}_\sigma^C = 0.2\%$ and $\mathcal{E}_\sigma^N = 1.6\%$, respectively. We obtain very similar results when we use other pairs of illuminations.

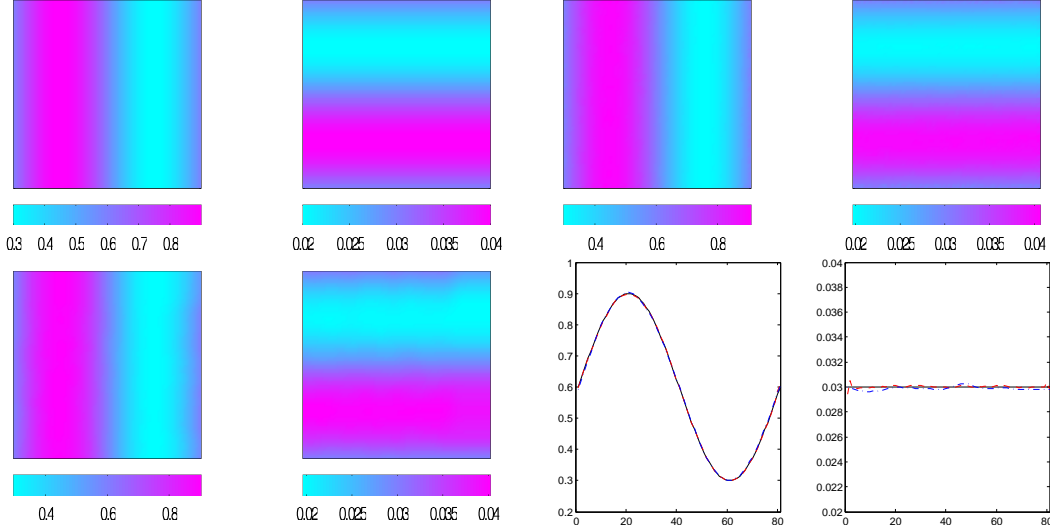


Figure 3: Experiment 3. From top left to bottom right are: true Γ and D , reconstructed Γ and D with noise-free data, reconstructed Γ and D with noisy data, cross-section of true (solid) and reconstructed (red dashed and blue dot-dashed) Γ and D along $y = 1$ with noisy data.

Experiment 3. In this experiment, we intend to reconstruct the Grüneisen and diffusion coefficients:

$$\Gamma(\mathbf{x}) = 0.6 + 0.3 \sin(\pi x) \quad \text{and} \quad D(\mathbf{x}) = 0.03 + 0.01 \sin(\pi y).$$

The absorption coefficient is the known constant $\sigma = 0.1$. The measurements are again constructed with the two sources g_1 and g_2 . The results of the numerical experiments are shown in Fig. 3. The relative L^2 errors in the reconstructions are $\mathcal{E}_\Gamma^C = 0.2\%$, $\mathcal{E}_\Gamma^N = 1.1\%$, $\mathcal{E}_D^C = 0.2\%$ and $\mathcal{E}_D^N = 1.4\%$, respectively. As can be seen from the cross-section plots, the reconstructions are fairly accurate. When noise-free data are used, we obtain almost perfect reconstructions.

Experiment 4. In this experiment, the absorption and diffusion coefficients are given by

$$\sigma(\mathbf{x}) = 0.1 + 0.2e^{-(x-1)^2 - (y-1)^2} \quad \text{and} \quad D(\mathbf{x}) = 0.03 + 0.02 \sin(\pi x) \sin(\pi y),$$

respectively. The Grüneisen coefficient is constant and given by $\Gamma = 0.5$. The measurements are constructed with the two sources g_1 and g_2 described above. The results of the numerical

experiment are shown in Fig. 4. The relative L^2 errors are $\mathcal{E}_\sigma^C = 0.2\%$, $\mathcal{E}_\sigma^N = 0.8\%$, $\mathcal{E}_D^C = 0.1\%$ and $\mathcal{E}_D^N = 3.1\%$, respectively.

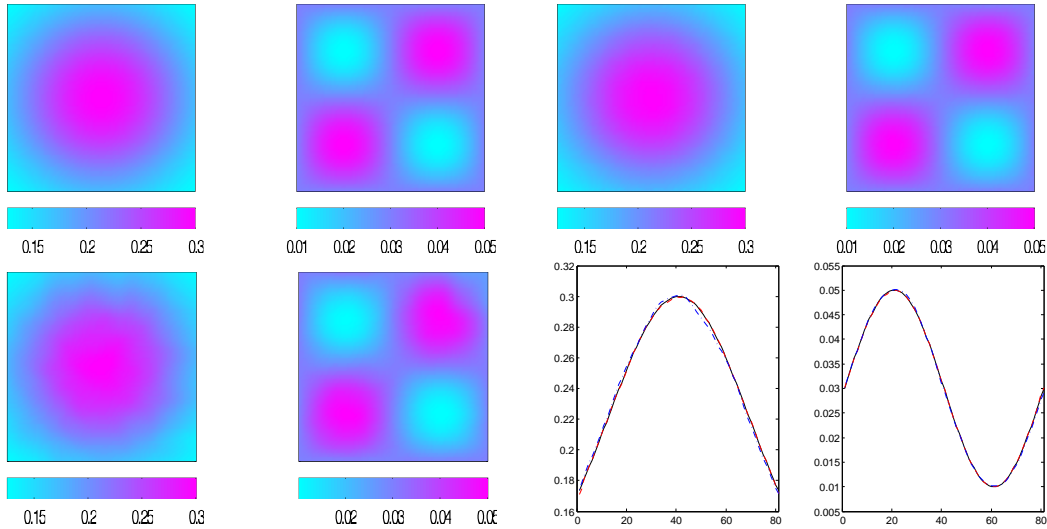


Figure 4: Experiment 4. From top left to bottom right are: true σ and D , reconstructed σ and D with noise-free data, reconstructed σ and D with noisy data, cross-section of true (solid) and reconstructed (red dashed and blue dot-dashed) σ and D along $y = 0.5$ with noisy data.

Numerical simulations with discontinuous coefficients. We now consider the reconstruction of discontinuous Grüneisen, absorption and diffusion coefficients. The reconstructions are done with the Bregman iteration method that was described above. As we have seen, the discontinuities in $\Gamma(\mathbf{x})$ and $\sigma(\mathbf{x})$ cause no problem in the reconstructions, while the discontinuities in the diffusion coefficient require special treatment.

Experiment 5. In this experiment, we intend to reconstruct the Grüneisen coefficient that contains three inclusions at $X_1 = [0.3 \ 0.7] \times [0.3 \ 0.7]$, $X_2 = [0.8 \ 1.2] \times [1.3 \ 1.7]$ and $X_3 = [1.3 \ 1.7] \times [0.3 \ 1.1]$ and a smooth absorption coefficient:

$$\Gamma(\mathbf{x}) = \begin{cases} 0.8, & \mathbf{x} \in X_1 \cup X_2 \\ 0.4, & \mathbf{x} \in X \setminus (X_1 \cup X_2) \end{cases} \quad \text{and} \quad \sigma(\mathbf{x}) = \begin{cases} 0.3, & \mathbf{x} \in X_3 \\ 0.1, & \mathbf{x} \in X \setminus X_3. \end{cases}$$

The diffusion coefficient is a known constant $D(\mathbf{x}) = 0.02$. The measurements are constructed with the same sources as in Experiment 1. The results of the numerical experiment are shown in Fig. 5. The relative L^2 errors in the reconstructions are $\mathcal{E}_\Gamma^C = 0.2\%$, $\mathcal{E}_\Gamma^N = 5.0\%$, $\mathcal{E}_\sigma^C = 0.2\%$ and $\mathcal{E}_\sigma^N = 10.7\%$, respectively. Inside each region of constant coefficients, the reconstructions are as accurate as before. The error in the reconstructions occurs mainly at the location of the discontinuities. Even so, the jump of the coefficients across the interface is well captured.

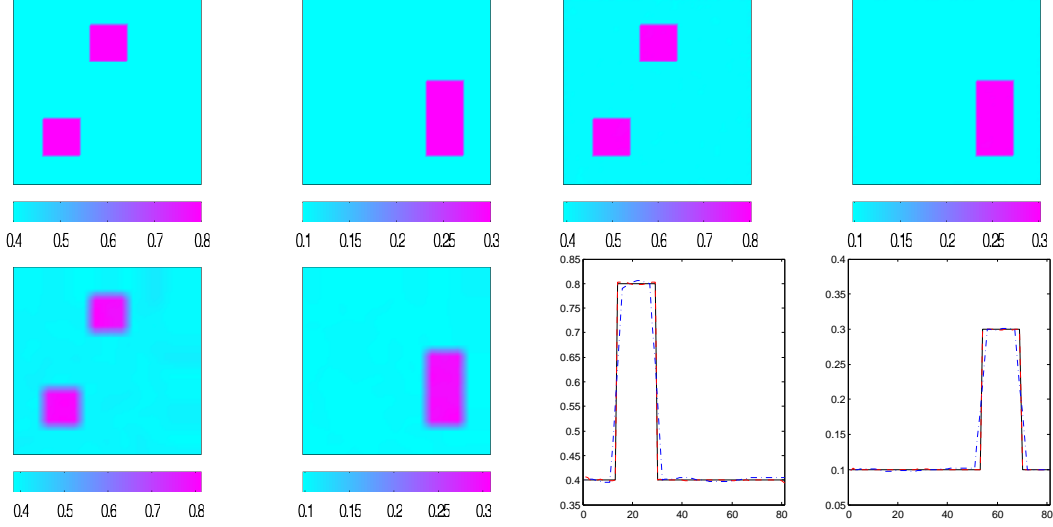


Figure 5: Experiment 5. From top left to bottom right: true Γ and σ , reconstructed Γ and σ with noise-free data, reconstructed Γ and σ with noisy data, cross-section of true (solid) and reconstructed (red dashed and blue dot-dashed) Γ and σ along $y = 0.5$ with noisy data.

Experiment 6. In this experiment, we intend to reconstruct the discontinuous Grüneisen and diffusion coefficients:

$$\Gamma(\mathbf{x}) = \begin{cases} 0.3, & \mathbf{x} \in X_1 \\ 0.1, & \mathbf{x} \in X \setminus X_1 \end{cases} \quad \text{and} \quad D(\mathbf{x}) = \begin{cases} 0.04, & \mathbf{x} \in X_2 \cup X_3 \\ 0.02, & \mathbf{x} \in X \setminus (X_2 \cup X_3). \end{cases}$$

The absorption coefficient is a known constant $\sigma(\mathbf{x}) = 0.1$. The measurements are constructed with the same two sources g_1 and g_2 as in the previous cases. The results of the numerical experiment are shown in Fig. 6. The relative L^2 errors in the reconstructions are $\mathcal{E}_\sigma^C = 0.2\%$, $\mathcal{E}_\sigma^N = 6.2\%$, $\mathcal{E}_D^C = 0.2\%$ and $\mathcal{E}_D^N = 7.1\%$, respectively.

Experiment 7. In this experiment, we intend to reconstruct the absorption coefficient

$$\sigma(\mathbf{x}) = \begin{cases} 0.1 + 0.1 * (\text{sign}(\text{random}) + 1), & \mathbf{x} \in X_{ij}, 1 \leq i, j \leq 10 \\ 0.1, & \mathbf{x} \in X \setminus (\cup X_{i,j}), \end{cases}$$

where random is a random number in $[-1, 1]$ and X_{ij} is the box $X_{ij} = [0.3 + 0.1(i-1), 0.3 + 0.1i] \times [0.3 + 0.1(j-1), 0.3 + 0.1j]$, and the discontinuous diffusion coefficient

$$D(\mathbf{x}) = \begin{cases} 0.02 + 0.02 * (\text{sign}(\text{random}) + 1), & \mathbf{x} \in X_{ij}, 1 \leq i, j \leq 10 \\ 0.02, & \mathbf{x} \in X \setminus (\cup X_{i,j}) \end{cases}$$

where X_{ij} is the box $X_{ij} = [0.7 + 0.1(i-1), 0.7 + 0.1i] \times [0.7 + 0.1(j-1), 0.7 + 0.1j]$. The Grüneisen coefficient is a known constant $\Gamma(\mathbf{x}) = 0.5$. The measurements are constructed with the two sources g_1 and g_2 . One realization of the coefficients and the results of the numerical experiment are shown in Fig. 7. The relative L^2 error in the reconstructions are $\mathcal{E}_\sigma^C = 0.2\%$, $\mathcal{E}_\sigma^N = 13.0\%$, $\mathcal{E}_D^C = 0.2\%$ and $\mathcal{E}_D^N = 16.2\%$, respectively.

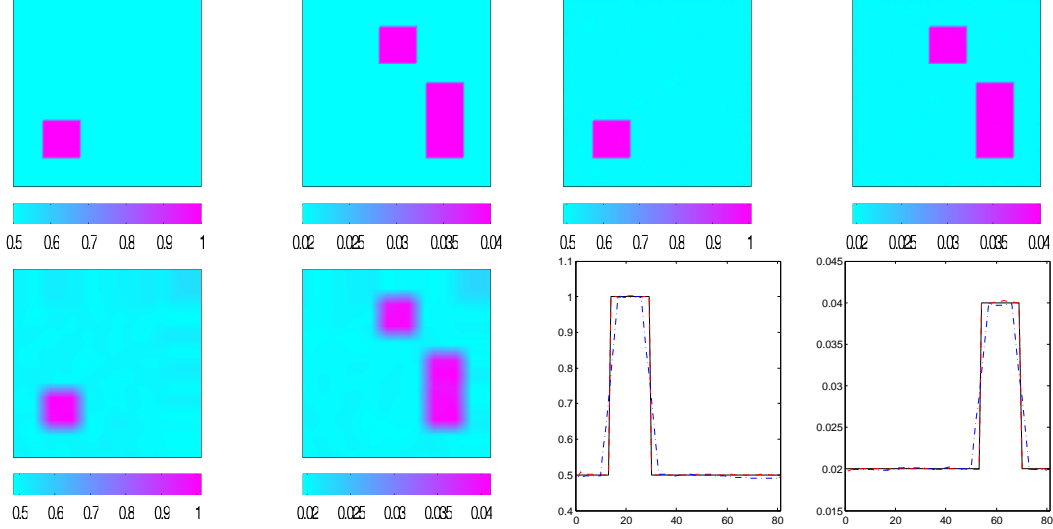


Figure 6: Experiment 6. From top left to bottom right are: true Γ and D , reconstructed Γ and D with noise-free data, reconstructed Γ and D with noisy data, cross-section of true (solid) and reconstructed (red dashed and blue dot-dashed) Γ and D along $y = 1$.

Numerical simulations with multiple illuminations. We have seen that multiple illuminations would not provide extra information that would allow us to reconstruct all three coefficients. However, acquiring more data does improve reconstructions by averaging out noise in the data.

Experiment 8. We present here a reconstruction of the absorption and diffusion coefficients of Experiment 6 with multiple data sets. We have a total of 10 measurements constructed using the sources g_1 - g_{10} , with g_1 - g_8 given above and g_9 , g_{10} given as

$$g_9 = \begin{cases} \frac{(y-1)^2}{e^{-\frac{(y-1)^2}{2 \cdot 0.1^2}}}, & \mathbf{x} \in \partial X_L, \\ 0.0, & \mathbf{x} \in \partial X \setminus \partial X_L \end{cases}, \quad g_{10} = \begin{cases} \frac{(y-1)^2}{e^{-\frac{(y-1)^2}{2 \cdot 0.1^2}}}, & \mathbf{x} \in \partial X_R, \\ 0.0, & \mathbf{x} \in \partial X \setminus \partial X_R. \end{cases}$$

The data are polluted again with 8% of random noise. The transport equations are solved in the least square sense with l^1 sparsity regularization using the Bregman iteration method. The reconstruction results are presented in Fig. 8. The relative L^2 error in the reconstructions are $E_\sigma^C = 0.1\%$, $E_\sigma^N = 9.3\%$, $E_D^C = 0.1\%$ and $E_D^N = 9.6\%$, respectively. The reconstructions from redundant measurements in the case of noisy data are indeed improved.

5 Conclusions

This paper considers the reconstruction of (D, σ, Γ) from knowledge of several measurements of the form $H_j(x) = \Gamma(x)\sigma(x)u_j(x)$, where the photon densities $u_j(x)$ solve the diffusion equation (1) with prescribed illuminations $g = g_j$ on ∂X for $1 \leq j \leq J$.

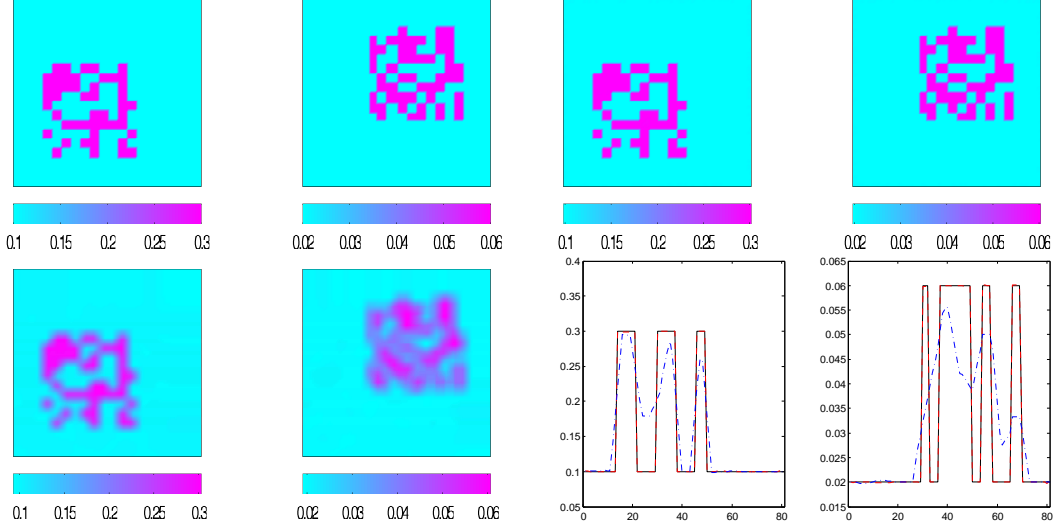


Figure 7: Experiment 7. From top left to bottom right are: true σ and D , reconstructed σ and D with noise-free data, reconstructed σ and D with noisy data, cross-section of true (solid) and reconstructed (red dashed and blue dot-dashed) σ and D along $y = 1$ with noisy data.

Our first main result is that independent of $J \geq 2$, the most we can obtain about (D, σ, Γ) are the two functionals (χ, q) defined in (6). In other words, knowledge of the full measurement operator \mathcal{H} , which to an arbitrary function g on ∂X associates $\mathcal{H}(g)(x) = \Gamma(x)\sigma(x)u(x)$ with u solution of (1), is equivalent to knowledge of (χ, q) .

The functionals (χ, q) are uniquely determined by two measurements (H_1, H_2) associated to well-chosen illuminations (g_1, g_2) . Solving for (χ, q) from knowledge of (H_1, H_2) requires that one solve an explicit linear transport equation (12) and then evaluate q in (13). That the illuminations are well-chosen means that the vector field β defined in (3) and appearing in (12) never vanishes so that (4) holds. A large class of such well-chosen illuminations exists in two dimensions of space as indicated in Lemma 2.1. In three dimensions of space, ensuring (4) independently of the unknown coefficients (D, σ, Γ) in a given set of admissible coefficients is much more difficult and the only methodology known at present is the one developed in [12] based on the construction of complex geometrical optics solutions.

Our second main result concerns the reconstructions of (D, σ, Γ) from knowledge of (χ, q) . We show in Corollary 2.3 that knowledge of (χ, q) and one coefficient in (D, σ, Γ) *uniquely* and *stably* determines the remaining two coefficients. Arguably the most practical result concerns the unique and stable reconstruction of (D, σ) when Γ is known (and typically modeled as a constant coefficient). Other reconstructions may also be envisaged, such as for instance the reconstruction of (D, σ, Γ) from knowledge of the (reduced) scattering coefficient $\sigma_s = \frac{1}{3D} - \sigma$ and of (χ, q) . Similar techniques to those developed in Corollary 2.3 are then likely to be useful for such reconstructions although we do not pursue this in detail here.

The reconstruction of all parameters in (D, σ, Γ) is therefore *not possible*, independently of the reconstruction method employed, without additional prior information. Assuming knowledge of one of the three parameters as we have done in this paper is probably the

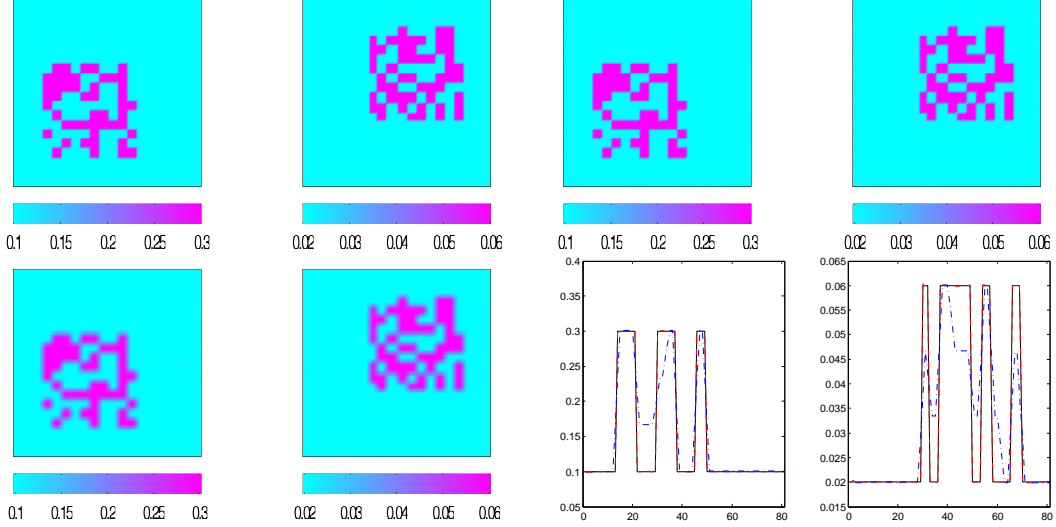


Figure 8: Experiment 8. From top left to bottom right are: true σ and D , reconstructed σ and D with noise-free data, reconstructed σ and D with noisy data, cross-section of true (solid) and reconstructed (red dashed and blue dot-dashed) σ and D along $y = 1$.

simplest model of prior information. Many other ways to incorporate prior information may be considered. We have mentioned the use of multiple frequencies (light colors) and a priori prescribed behaviors of the coefficients (D, σ) with respect to frequency as a means to address non-uniqueness; see e.g. [9]. Assuming the coefficients are piecewise constant may also help restore uniqueness since the expression for $q(x)$ in (6) may provide information about the jump of D across (smooth) interfaces. Prior information strategies (other than assuming one of the coefficients known) were not considered in this paper. They are, however, rendered necessary by the non-uniqueness results obtained in Theorem 2.2.

From the computational viewpoint, the reconstruction procedures require that we solve a transport equation of the form (12) to reconstruct $\chi(x)$ and possibly an elliptic equation of the form (10) or (11) to reconstruct $D(x)$. The simulation of all transport and elliptic equations was performed by using first-order Galerkin methods.

In the presence of smooth coefficients, we have observed almost no difference between the two regularization methods in (19) and (20) to solve the transport equation for χ . However, some care needs to be taken with the vector field β in the presence of discontinuous coefficients (D, σ, Γ). The two-dimensional numerical reconstructions performed with the l_1 minimization scheme (20) proved to be very robust with respect to the (not very physical) additive noise considered in (23). Reconstructions based on (19) or Tikhonov regularizations proved less robust.

More physical models of noise, including “noise” generated in the reconstruction of $H(x)$ from boundary pressure measurements (the first step of PAT mentioned in the introduction), still need to be derived. Since the proposed reconstruction methodology was able to handle the numerically more challenging high frequency component of the noise, we are confident that reconstructions based on e.g. (12)-(10) will prove quite robust with realistic noise models or experimental data.

Acknowledgment

We would like to thank the reviewers for several comments and suggestions that helped improve the presentation of our results. GB was supported in part by NSF Grants DMS-0554097 and DMS-0804696. KR was supported in part by NSF Grant DMS-0914825.

References

- [1] R. A. ADAMS, *Sobolev Spaces*, Academic Press, NY, San Francisco, London, 1975.
- [2] G. ALESSANDRINI, *An identification problem for an elliptic equation in two variables*, Ann. Mat. Pura Appl., 145 (1986), pp. 265–296.
- [3] L. AMBROSIO, *Transport equation and Cauchy problem for BV vector fields*, Invent. Math., 158 (2004), p. 227260.
- [4] H. AMMARI, E. BONNETIER, Y. CAPDEBOSCQ, M. TANTER, AND M. FINK, *Electrical impedance tomography by elastic deformation*, SIAM J. Appl. Math., 68 (2008), pp. 1557–1573.
- [5] H. AMMARI, E. BOSSY, V. JUGNON, AND H. KANG, *Mathematical models in photo-acoustic imaging of small absorbers*, SIAM Review, (2010).
- [6] S. R. ARRIDGE AND J. C. SCHOTLAND, *Optical tomography: forward and inverse problems*, Inverse Problems, 25 (2010), p. 123010.
- [7] G. BAL, *Inverse transport theory and applications*, Inverse Problems, 25 (2009), p. 053001.
- [8] G. BAL, A. JOLLIVET, AND V. JUGNON, *Inverse transport theory of Photoacoustics*, Inverse Problems, 26 (2010), p. 025011.
- [9] G. BAL AND K. REN, *On multi-spectral quantitative photoacoustic tomography*, submitted.
- [10] G. BAL, K. REN, G. UHLMANN, AND T. ZHOU, *Quantitative thermo-acoustics and related problems*, submitted.
- [11] G. BAL AND J. C. SCHOTLAND, *Inverse Scattering and Acousto-Optics Imaging*, Phys. Rev. Letters, 104 (2010), p. 043902.
- [12] G. BAL AND G. UHLMANN, *Inverse diffusion theory for photoacoustics*, Inverse Problems, 26(8) (2010), p. 085010.
- [13] F. BOUCHUT AND G. CRIPPA, *Uniqueness, renormalization and smooth approximations for linear transport equations*, SIAM J. Math. Anal., 38 (2006), pp. 1316–1328.
- [14] Y. CAPDEBOSCQ, J. FEHRENBACH, F. DE GOURNAY, AND O. KAVIAN, *Imaging by modification: numerical reconstruction of local conductivities from corresponding power density measurements*, SIAM J. Imaging Sciences, 2 (2009), pp. 1003–1030.
- [15] F. COLOMBINI, G. CRIPPA, AND J. RAUCH, *A note on two-dimensional transport with bounded divergence*, Comm. Partial Differential Equations, 31 (2006), pp. 1109–1115.

- [16] F. COLOMBINI AND N. LERNER, *Uniqueness of continuous solutions for BV vector fields*, Duke Math. J., 111 (2002), p. 357384.
- [17] B. T. COX, S. R. ARRIDGE, AND P. C. BEARD, *Estimating chromophore distributions from multiwavelength photoacoustic images*, J. Opt. Soc. Am. A, 26 (2009), pp. 443–455.
- [18] B. T. COX, J. G. LAUFER, AND P. C. BEARD, *The challenges for quantitative photoacoustic imaging*, Proc. of SPIE, 7177 (2009), p. 717713.
- [19] ———, *Quantitative photoacoustic image reconstruction using fluence dependent chromophores*, Biomedical Optics Express, 1(1) (2010), pp. 201–208.
- [20] R. J. DIPERNA AND P.-L. LIONS, *On the cauchy problem for boltzmann equations: global existence and weak stability*, Ann. of Math. (2), 130 (1989), pp. 321–366.
- [21] D. FINCH AND RAKESH., *Recovering a function from its spherical mean values in two and three dimensions*, in Photoacoustic imaging and spectroscopy L. H. Wang (Editor), CRC Press, (2009).
- [22] S. K. FINCH, D. PATCH AND RAKESH., *Determining a function from its mean values over a family of spheres*, SIAM J. Math. Anal., 35 (2004), pp. 1213–1240.
- [23] A. R. FISHER, A. J. SCHISLER, AND J. C. SCHOTLAND, *Photoacoustic effect for multiply scattered light*, Phys. Rev. E, 76 (2007), p. 036604.
- [24] H. GAO, H. ZHAO, AND S. OSHER, *Bregman methods in quantitative photoacoustic tomography*. CAM Report 10-42, UCLA, 2010.
- [25] D. GILBARG AND N. S. TRUDINGER, *Elliptic Partial Differential Equations of Second Order*, Springer-Verlag, Berlin, 1977.
- [26] M. HAURAY, *On two-dimensional Hamiltonian transport equations with L^p_{loc} coefficients*, Ann. IHP. Anal. Non Lin., 20 (2003), p. 625644.
- [27] Y. HRISTOVA, P. KUCHMENT, AND L. NGUYEN, *Reconstruction and time reversal in thermoacoustic tomography in acoustically homogeneous and inhomogeneous media*, Inverse Problems, 24 (2008), p. 055006.
- [28] R. KOWAR AND O. SCHERZER, *Photoacoustic imaging taking into account attenuation*, in Mathematics and Algorithms in Tomography, vol. 18, Mathematisches Forschungsinstitut Oberwolfach, 2010, pp. 54–56.
- [29] P. KUCHMENT AND L. KUNYANSKY, *Mathematics of thermoacoustic tomography*, Euro. J. Appl. Math., 19 (2008), pp. 191–224.
- [30] L. A. KUNYANSKY, *Explicit inversion formulae for the spherical mean radon transform*, Inverse Problems, 23 (2007), pp. 373–383.
- [31] J. R. MCCLAUGHLIN AND J. YOON, *Unique identifiability of elastic parameters from time-dependent interior displacement measurement*, Inverse Problems, 20 (2004), p. 2545.
- [32] A. NACHMAN, A. TAMASAN, AND A. TIMONOV, *Conductivity imaging with a single measurement of boundary and interior data*, Inverse Problems, 23 (2007), pp. 2551–2563.

- [33] A. NACHMAN, A. TAMASAN, AND A. TIMONOV, *Recovering the conductivity from a single measurement of interior data*, *Inverse Problems*, 25 (2009), p. 035014.
- [34] S. OSHER, M. BURGER, D. GOLDFARB, J. XU, AND W. YIN, *An iterative regularization method for total variation based image restoration*, *Multiscale Model. Simul.*, 4 (2005), pp. 460–489.
- [35] S. PATCH AND O. SCHERZER, *Photo- and thermo- acoustic imaging*, *Inverse Problems*, 23 (2007), pp. S1–10.
- [36] G. R. RICHTER, *An Inverse Problem for the Steady State Diffusion Equation*, *SIAM J. Applied Math.*, 41 (1981), pp. 210–221.
- [37] J. RIPOLL AND V. NTZIACHRISTOS, *Quantitative point source photoacoustic inversion formulas for scattering and absorbing medium*, *Phys. Rev. E*, 71 (2005), p. 031912.
- [38] P. STEFANOV AND G. UHLMANN, *Thermoacoustic tomography with variable sound speed*, *Inverse Problems*, 25 (2009), p. 075011.
- [39] F. TRIKI, *Uniqueness and stability for the inverse medium problem with internal data*, *Inverse Problems*, 26 (2010), p. 095014.
- [40] L. V. WANG, *Ultrasound-mediated biophotonic imaging: a review of acousto-optical tomography and photo-acoustic tomography*, *Journal of Disease Markers*, 19 (2004), pp. 123–138.
- [41] M. XU AND L. V. WANG, *Photoacoustic imaging in biomedicine*, *Rev. Sci. Instr.*, 77 (2006), p. 041101.
- [42] R. J. ZEMP, *Quantitative photoacoustic tomography with multiple optical sources*, *Applied Optics*, 49 (2010), pp. 3566–3572.